American Journal of Materials Science 2015, 5(2): 31-40
DOI: 10.5923/j.materials.20150502.02

Kinetic and Adsorption Behaviour of Aqueous Fe^{2+}, Cu^{2+} and Zn^{2+} Using a 30 nm Hydroxyapatite Based Powder Synthesized via a Combined Ultrasound and Microwave Based Technique

Sridevi Brundavanam, Gérrard Eddy Jai Poinern*, Derek Fawcett

Murdoch Applied Nanotechnology Research Group, Department of Physics, Energy Studies and Nanotechnology, School of Engineering and Energy, Murdoch University, Murdoch, Australia

Abstract The present study reports the kinetic and absorption performance of novel nanometre scale hydroxyapatite (HAP) absorber synthesised from a combined ultrasound and microwave based technique for the removal of metal ions (Fe^{2+}, Cu^{2+} and Zn^{2+}) from aqueous solutions. After powder characterisation was carried out using XRD, SEM, EDS and FT-IR, batch adsorption studies were carried out. Kinetic studies established that $Fe^{2+}$and Cu^{2+} ion adsorption tended to follow a pseudo-second order model, while Zn^{2+} ion adsorption tended to follow an intra-particle diffusion pattern. All three metal ion adsorption studies indicated an ion-exchange mechanism (metal ion → Ca^{2+}) was a primary participant in the sorption process and was influenced by intra-particle diffusion. The Isotherm studies indicated the Langmuir isotherm modelled Fe^{2+} and Cu^{2+} ion adsorption, while the Freundlich isotherm was the better model for Zn^{2+} ion adsorption data. Maximum adsorption capacity of HAP determined via Langmuir isotherm was found to be 61.35 mg/g for Cu^{2+} ions, 55.25 mg/g for Fe^{2+} ions and 48.54 mg/g for Zn^{2+} ions. The study established HAP as an effective absorbent material for the removal of Fe^{2+}, Cu^{2+} and Zn^{2+} loaded aqueous solutions.

Keywords Hydroxyapatite, Adsorption, Metal ion, Ultrasound, Microwaves

1. Introduction

The presence of heavy metal contaminants in the environment is a well-recognised problem that threatens the world today. Even in small concentrations, their high solubility in aquatic environments makes them extremely hazardous to living organisms [1, 2]. Once heavy metals enter the food chain their toxicity together with their tendency to accumulate beyond acceptable concentrations in the human body can result in serious health disorders [3]. Metals are generally considered heavy metals when their density exceeds 5 gcm^{-3} [4]. Metals and alloys with densities greater than 5 g cm^{-3} are widely used as biomaterials due to their superior mechanical properties. The majority of these metallic biomaterials are used in load-bearing implants such as bone plates, fixation pins and screws, hip and knee replacements. Metallic biomaterials are grouped into three distinct categories: 1) stainless steels; 2) cobalt-based alloys, and 3) titanium alloys. Individually, each category consists of a primary metallic biomaterial that is composed of a number of secondary metallic constituents. For example, the main constituents of stainless steels are iron (Fe), chromium (Cr) and nickel (Ni). Most of the metal constituents used in the three metallic biomaterial groups like Cr, cobalt (Co), Fe, molybdenum (Mo), Ni, and tungsten (W) are used as alloying elements to improve the properties of the main constituent element [5]. For example, Fe based stainless steels have Cr (17-20%) added to improve corrosion resistance and Mo (2-4%) is added to improve resistance to pitting corrosion [6]. However, metallic constituents such as Cr and Mo are toxic and can only be tolerated in very small amounts in the body. Studies have shown that leaching of metallic surgical implants can result in the release of toxic metallic ions into surrounding cells, blood vessels and tissues [7-9]. The release of metallic ions can only be tolerated in very minute amounts, as in larger amounts they induce an unfavourable inflammatory response that significantly reduces the biocompatibility of the implant [8]. Importantly, exposure to heavy metals can lead to serious health problems such as cancer, nervous system and organ damage. For example, both Cr and Ni are known carcinogens and long-term exposure can lead to the development and growth of cancer.

* Corresponding author:
G.Poinern@murdoch.edu.au (Gérrard Eddy Jai Poinern)
Published online at http://journal.sapub.org/materials

Metallic biomaterials used in orthopaedic applications will generally experience load-induced stresses in the inner core of the implant. Whereas, the surface of the implant is exposed to the surrounding physiological environment in the body. The interaction between exposed surface and physiological environment is very important in soliciting a favourable biological response. Because of the importance that biocompatibility plays in delivering a successfully implantation procedure, there have numerous studies into improving interfacial properties between the implant surface and the physiological environment [9, 10]. To this end, bioactive coatings based on calcium phosphate ceramics have been extensively investigated and used to coat a variety of biomedical metallic implants. These coatings have been found to improve biocompatibility, promote implant attachment and restrain the release of metallic ions into the physiological environment [10, 12]. In particular, hydroxyapatite (HAP) is a thermodynamically stable mineral phase at physiological pH and has a hexagonal crystal structure composed of calcium phosphate groups. Both crystallographic and chemical studies reveal synthetic HAP is similar in chemical composition to the naturally occurring mineral phase found in human bone and teeth [13]. Synthetic HAP has the advantages of being biocompatible, non-toxic, and has enhanced bioactive properties towards bone cells and other body tissues [14].

Another interesting property of HAP results from its complex hexagonal structure. The structure provides effective high capacity absorbance for a variety of pharmaceutical products such as antibiotics, drugs, enzymes, hormones and steroids. The use of HAP as a slow and sustained release drug delivery platform has proven to be effective in the treatment of diseases such as osteomyelitis, osteoporosis and osseous cancer [15-18]. Likewise, HAP used in orthopaedic applications also has the potential to act as an adsorption matrix. In this case, adsorption results from a mass transfer process by which metallic particles are transferred from the physiological environment (liquid phase) to the HAP matrix, and become bound by physical and/or chemical interactions. HAP makes an attractive absorbent because of its advantageous surface properties such as its hydrophilic nature, surface charge, pH, porous structure and 2.6 P-OH surface groups per nm^2 which act as sorption sites [19, 20]. Generally speaking there are three steps involved in sorption of metallic particles onto the HAP absorber: (1) transfer of metallic ion particles from the physiological environment to the absorber surface; (2) adsorption on the metallic ion particles onto the surface, and (3) transport of the metallic ion particles within the absorber matrix.

In the present work the adsorption of copper (Cu), iron (Fe), and zinc (Zn) ions from aqueous solutions onto a solid nanometre scale HAP powder in agitated batch absorber vessels was studied. The nanometre scale HAP powder was synthesized via a combined ultrasound and microwave based technique to produce a spherical particle with a mean diameter of 30 nm. The main goal of this study was to examine the ability of the nanometre scale HAP powder to remove these ions from an aqueous solution and therefore evaluate its potential to store heavy metallic ions. The source of these metallic ions could arise from the corrosion and wear of surgical implants or by metabolic uptake via nutritional intake, drinking water and inhalation. The synthesized HAP powders were characterized using X-ray diffraction (XRD) spectroscopy, Scanning electron microscopy (SEM), Energy Dispersive Spectroscopy (EDS) and Fourier Transform Infrared Spectroscopy (FTIR). The metal ion adsorption capacity of the powders were investigated via the removal of Cu, Fe, and Zn ions from aqueous solutions using a batch equilibrium procedure. The kinetic behaviour of metal ion adsorption was investigated using Lagergren's pseudo-first order, McKay & Ho's pseudo-second order and intra-particle diffusion models. Furthermore, Langmuir and Freundlich adsorption isotherms were used to model the experimental data.

2. Materials and Methods

2.1. Materials

Adsorption experiments were conducted using three different metal salts. The first, $FeCl_2.4H_2O$ was supplied by Chem-Supply (Australia). The second, $CuCl_2.2H_2O$ was supplied by Sigma-Aldrich (United States) and the third, $ZnCl_2$ was supplied by Scharlau (Barcelona, Spain). Each respective metal salt was dissolved in an aqueous solution to make up a 1000 ppm stock solution and lower solution concentrations were produced by successive dilution of the stock solution. HAP powders were synthesized from high purity calcium nitrate tetra-hydrate [$Ca(NO_3)_2.4H_2O$] and potassium di-hydrogen phosphate [KH_2PO_4], while solution pH was controlled by the addition of ammonium hydroxide [NH_4OH]. All chemicals used to synthesize HAP were supplied by Chem-Supply (Australia). During HAP synthesis an Ultrasound Processor [UP50H: 50 W, 30 kHz, MS7 Sonotrode (7mm diameter, 80 mm length)] supplied by Hielscher Ultrasound Technology was used to deliver the ultrasound irradiation. All aqueous solutions were made using Milli-Q® water (18.3 MΩ cm^{-1}) produced by an ultrapure water system (Barnstead Ultrapure Water System D11931; Thermo Scientific, Dubuque, IA).

2.2. Synthesis of Nanometres Scale Hydroxyapatite

Ultrasonic and microwave processing are two techniques that significantly influence and enhance the properties of materials. Ultrasound produces extremely rapid pressure and temperature variations that promote both physical effects and chemical reactions that directly influence particle size and morphology during synthesis. Microwave processing has the advantages of providing controlled volumetric heating, lower energy consumption, reduced reaction times, increased product yields, and improved material properties when compared to conventional heating methods [21]. A detailed synthesis procedure developed by

the authors is given elsewhere [21, 22]. But a brief description is give here in the interest of completeness and begins by adding a 40 mL solution of 0.32 M calcium nitrate tetra-hydrate into a small glass beaker. The pH of the solution is then adjusted to 9.0 by adding approximately 2.5 mL of ammonium hydroxide. The solution was then subjected to 50 W of ultrasound irradiation for 1 h set and maximum amplitude. The second hour of ultrasound treatment included slowly adding 60 mL of 0.19 M potassium di-hydrogen phosphate solution. During the addition of potassium di-hydrogen phosphate the solution pH was maintained at 9.0 and the Calcium/Phosphate [Ca/P] ratio was maintained at 1.67. After ultrasonic treatment, the solution was centrifuged (15,000 g) for 20 minutes at room temperature to produce a solid white precipitate. The precipitate was collected, washed and centrifuged for a further 10 minutes. At the end of the second centrifugation, the precipitate was placed into a fused silica crucible and then loaded into a domestic microwave oven for thermal treatment [Set at 100% power for 40 minutes: 1100W at 2450 MHz-LG® Australia] [21]. The resultant agglomerated powder was collected and then subjected to ball milling until an ultrafine nanometre scale HAP powder was produced.

2.3. Advanced Characterisation Techniques

2.3.1. X-ray Diffraction (XRD) Spectroscopy

XRD spectroscopy was used to study the synthesized powders, with the XRD patterns being used to identify the crystalline size and phases present. Spectroscopy data was recorded at room temperature, using a Siemens D500 series diffractometer [Cu Kα = 1.5406 Å radiation source] operating at 40 kV and 30 mA. The diffraction patterns were collected over a 2θ range of 20° to 60° with an incremental step size of 0.04° using flat plane geometry with 2 second acquisition time for each scan. The scan data was then used in conjunction with the Debye-Scherrer equation [Equation 1] to determine the crystalline size of each sample.

2.3.2. Scanning Electron Microscopy (SEM) and Energy Dispersive Spectroscopy (EDS)

The SEM technique was used to examine the size, shape and morphological features of absorbents before and after the batch adsorption studies. All micrographs were taken using a JCM-6000, NeoScopeTM with attached energy dispersive X-ray spectroscopy. Samples were mounted on individual substrate holders using carbon adhesive tape before being sputter coated with a 2 nm layer of gold to prevent charge build up using a Cressington 208HR High Resolution Sputter coater.

2.3.3. Fourier Transform Infrared Spectroscopy (FT-IR)

FT-IR spectroscopy was used to identify species and functional groups present in the HAP absorber before and after metal adsorption studies. Samples were examined using a Perkin–Elmer Frontier FT-IR spectrometer with Universal Single bounce Diamond ATR attachment. Both FT-IR spectra were recorded in the range from 525 to 4000 cm^{-1} in steps of 4 cm^{-1}.

2.4. Batch Adsorption Studies

All adsorption experiments were carried out using the batch equilibrium technique. During the experimental work the adsorption capacity of the HAP absorber for three metal ions, namely, Cu^{2+}, Fe^{2+} and Zn^{2+} were investigated. The study also examined the influence of the initial metal ion concentration and contact time at 298ºC. The influence of contact time on metal ion adsorption on the absorber was examined using aqueous solutions containing 300 mg/L of metal ions (300 ppm) prepared from the three metal chlorides. HAP samples (0.1 g) were taken from the stock solution (1g/L) were added to each of the 300 ppm metal chloride solutions. The magnetic stirring speed for each metal suspension were set to 400 rpm, while the temperature of each suspension was maintained at 298 ± 1 K. In addition, the initial and final pH of the suspensions were recorded. Sample volumes were taken from the suspension during the mixing process at pre-determined time intervals (10, 20, 30, 40, 60, 90, 120, 180, 240 and 300 min) so that metal ion concentration in the respective solution could be measured. Once a sample volume was taken, an equivalent volume was added to maintain testing solution volume. Each solution volume was filtered using a Whatman® 0.22μm membrane syringe filter before being centrifuged at 15,000 g for 20 minutes. The concentration of Cu^{2+}, Fe^{2+}, Zn^{2+} and Ca^{2+} ions in the sample solutions were determined using atomic absorption spectroscopy (AAS). The instrument used was a Varian SpectrAA50 (Victoria, Australia) flame atomic absorption spectrometer operated in accordance with the manufacturer's recommendations. Elemental analysis of Cu, Fe and Zn was carried out using an air–acetylene flame and Ca analysis was carried using a nitrous oxide (N_2O)–acetylene flame. Sample aspiration flow rate used was 5 mL min−1. During analysis hollow cathode lamps of Fe, Cu, Zn and Ca (Varian) were used. While Fe, Cu, Zn and Ca concentration were measured at the wavelengths of 248.3, 324.8, 213.9 and 422.7 nm respectively. In addition, the influence of initial metal ion concentration was studied by first preparing a series of Schott reagent bottles containing 100 mL aqueous solutions consisting of varying concentrations of metal ions (100, 150, 200, 250 and 300 mg/L). All initial metal ion concentration experiments were carried out in triplicate. The data collected from the adsorption experiments were then used in the subsequent kinetic and adsorption isotherm modelling studies.

3. Results and Discussions

3.1. XRD Spectroscopy, SEM and EDS Analysis

XRD spectroscopy was carried out on all HAP powders

before and after adsorption studies. The resultant XRD patterns were used to determine crystalline size and phases present in the samples. An XRD pattern of a typical pure powder sample before adsorption testing is presented in Figure 1 and is indicated by the purple pattern. Examination of the pure HAP sample pattern reveals the presence of peaks that coincide with the known phases of pure HAP and is consistent with the phases listed in the ICDD database. The main (h k l) indices found in pure HAP, namely (002), (211), (112), (300), (202), (310), (222), (213) and (004) can be seen in the pattern for the synthesized HAP powder. In addition, the pattern showed no evidence of non-HAP phases. The crystalline size, $t_{(hkl)}$, of each sample was calculated from the respective XRD patterns using the Debye-Scherrer equation [23-25]

$$t_{(hkl)} = \frac{0.9\lambda}{B\cos\theta_{(hkl)}} \quad (1)$$

where, λ is the wavelength of the monochromatic X-ray beam, B is the Full Width at Half Maximum (FWHM) of the peak at the maximum intensity, $\theta_{(hkl)}$ is the peak diffraction angle that satisfies Bragg's law for the (h k l) plane and $t_{(hkl)}$ is the crystallite size. The mean crystallite size calculated from the (002) reflection peak for pure HAP sample was found to be 30 nm.

After adsorption studies, XRD spectroscopy was carried out on the metal ion loaded samples and representative XRD patterns are presented in Figure 1. XRD analysis reveals that there was no major changes in peak locations and powder size resulting from metal ion adsorption, as seen in Figure 1. To investigate this result further, SEM and EDS analysis was carried out on all samples. SEM analysis revealed that all powder samples displayed the same agglomerated spherical and granular morphology.

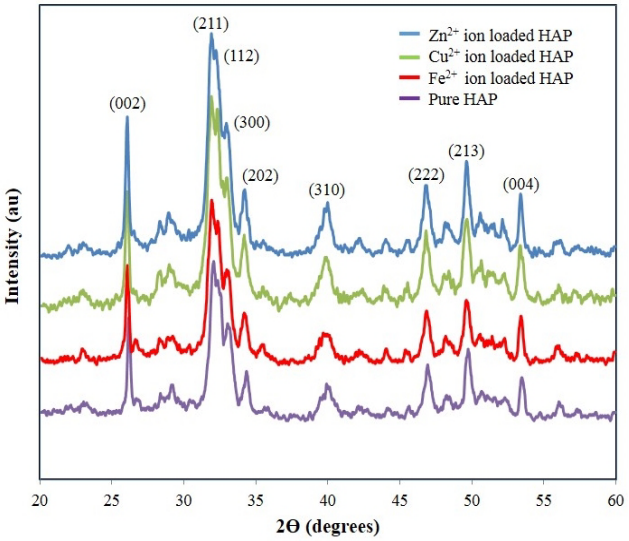

Figure 1. XRD patterns of powder samples before and after adsorption studies. The lower (Purple) pattern is a typical unloaded HAP powder sample, while the second (Red) a Fe^{2+} loaded sample. This is followed by a Cu^{2+} (Green) loaded sample and finally a Zn^{2+} (Blue) loaded sample

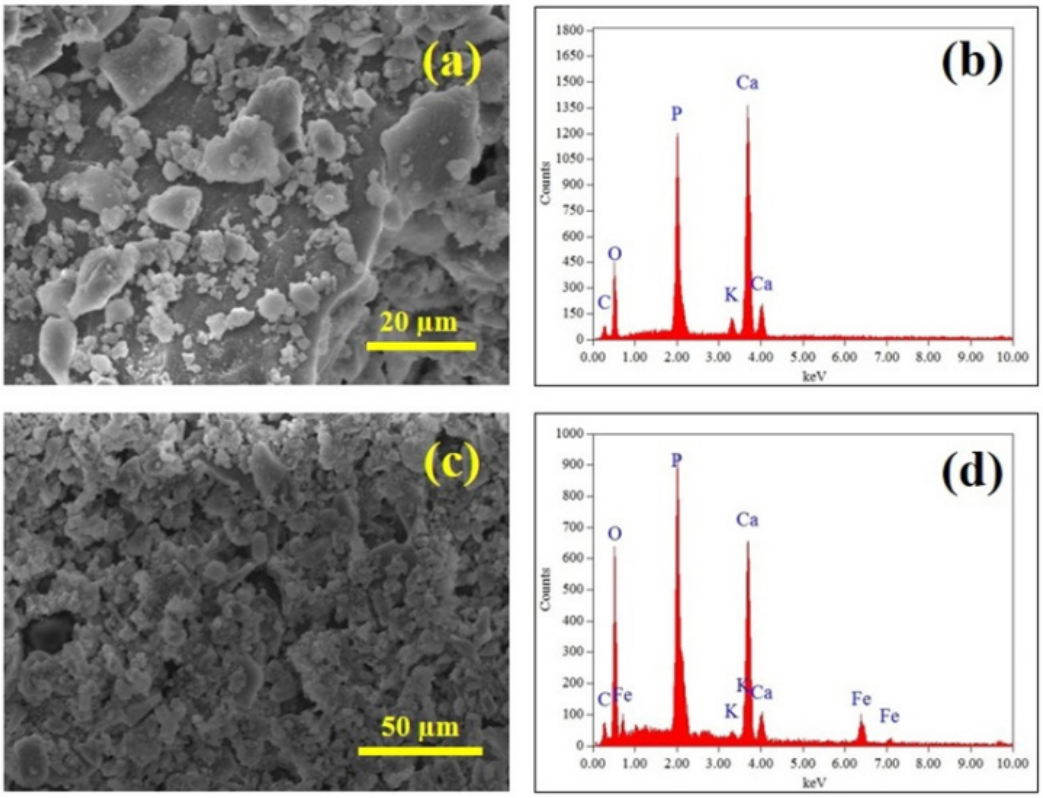

Figure 2. (a) SEM of a pure HAP powder; (b) EDS of pure HAP sample with a Ca:P ratio of 1.66; (c) SEM micrograph of an Fe^{2+} loaded sample, and (d) EDS spectrum confirming the presence of Fe^{2+} ions in the powder sample

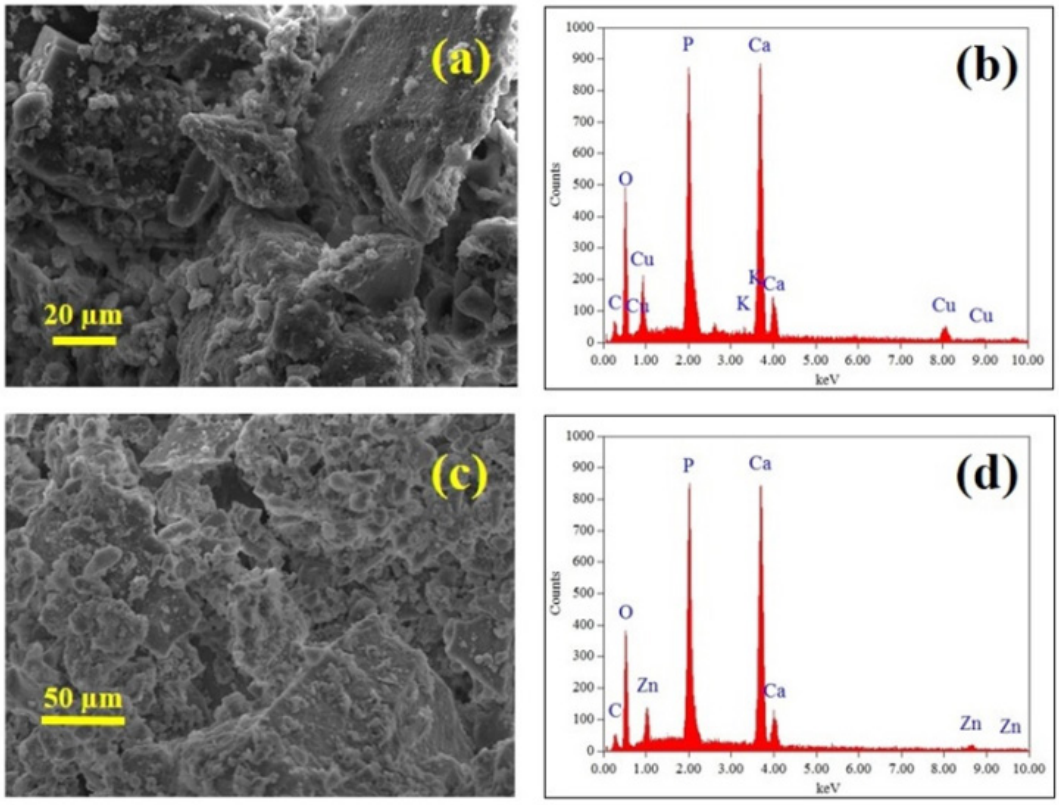

Figure 3. (a) SEM micrograph of Cu^{2+} loaded sample; (b) EDS spectrum of Cu^{2+} loaded sample; (c) SEM micrograph of an Zn^{2+} loaded sample, and (d) EDS spectrum confirming the presence of Zn^{2+} ions

Figure 2 (b) presents a typical EDS spectrum of an unloaded sample showing dominant peaks corresponding to Ca, P, and O, and confirms the chemical composition of HAP. Analysis of the EDS data revealed a Ca:P ratio of 1.66, which was very close to the ideal value of 1.67 normally associated with HAP. Also present was a minor peak that resulted from the carbon adhesive tape used to attach the sample to the SEM stub. Figure 2 (c) presents an SEM micrograph of a representative Fe^{2+} loaded sample that also displays the highly agglomerated nature of the synthesized powder. The accompanying EDS spectrum confirms the presence of Fe^{2+} ions present in the sample. The EDS also shows that there has been a reduction in the intensity of the Ca peak and suggests Fe^{2+} ions have replaced Ca^{2+} ions in the lattice. Studies have shown that divalent metal cations have a strong selectivity towards the Ca^{2+} in the HAP lattice via an ion-exchange mechanism [26, 27]. A similar trend can be seen for Cu^{2+} and Zn^{2+} ion load samples as seen in Figure 3. However, the reduction in the Ca peak for the Cu^{2+} and Zn^{2+} ion load samples is not as pronounced as the Fe^{2+} loaded sample seen in Figure 2 (d). The ion-exchange mechanism between the respective metal ion and Ca^{2+} can be represented by the equivalent molar exchange in the general HAP formula Ca_{10-x} $Mx(PO_4)_6$ $(OH)_2$, where M represents the respective metal ion and x can vary from 0 to 10 depending on experimental parameters and reaction time. Studies reported in the literature have detected very small XRD shifts associated with the ion-exchange mechanism for divalent metal ions [26, 28]. Inspection of the XRD patterns of representative metal ion loaded samples presented in Figure 1 do not reveal any of these very small XRD shifts.

3.2. FT-IR Spectroscopy Studies

FT-IR spectroscopy was used to detect species and functional groups associated with peaks seen in sample spectra taken before and after adsorption studies. Figure 4 presents the results of a FT-IR spectroscopy study of HAP powder samples taken before and after metal ion adsorption studies. Starting from the right hand side of Figure 4 with a typical synthesized HAP powder sample (purple) prior to adsorption studies. The first three peaks encountered are 561 cm^{-1}, 600 and 631cm^{-1} that are associated with $\nu 4$ vibrations of the O-P-O modes. The peak located at 827 cm^{-1} indicates the presence of carbonates in the sample and is a consequence of atmospheric carbon dioxide interacting with HAP precursors during synthesis and has been reported in the literature by other researchers [29, 30]. The small peak located at 963 cm^{-1} is associated with $\nu 1$ symmetric stretching vibrations associated with a P-O mode. While the much larger peak at 1026 cm^{-1} and the smaller peak located at 1090 cm^{-1} correspond to PO_4^{3-} functional groups. While the peaks located at 1373 cm^{-1} and 1643 cm^{-1} correspond to CO_3^{2-} functional groups. While the weak peak located at 3470 cm^{-1} corresponds to OH^- ion vibrations in the HAP crystal lattice. The three remaining spectra are

representative Fe^{2+}, Cu^{2+} and Zn^{2+} loaded powder samples taken after adsorption testing. The results for the metal ion loaded samples are very much the same as the pre-adsorption sample, except that both 872 cm^{-1} and 1373 cm^{-1} peak intensities have vanished from all spectra. Both the missing peaks correspond to CO_3^{2-} functional groups and suggest that the low pH of the batch adsorption technique resulted in the loss of the carbonates. For example, equilibrium pH of the Fe^{2+} ion and HAP solution pH was 3.2, while Cu^{2+} was 3.8 and Zn^{2+} was 4.4.

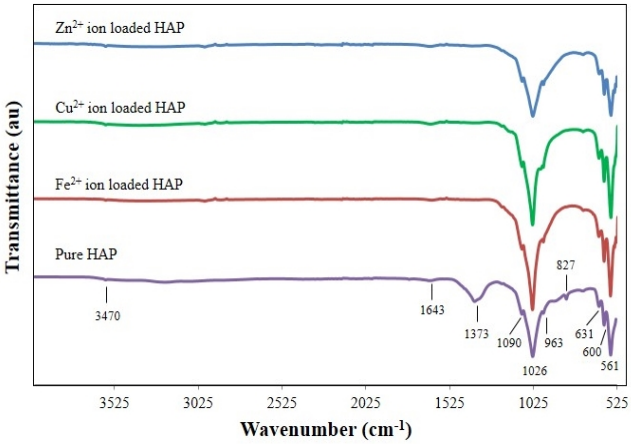

Figure 4. FT-IR Spectroscopy analysis of synthesized pure nanometre scale hydroxyapatite powder and metal ion loaded samples after adsorption studies

3.3. Adsorption Kinetics

A proper understanding of adsorption kinetics is important since sufficient residence time on the absorber surface is needed to complete the adsorption reaction. This is reflected in the metal ion concentration profiles encountered during the batch adsorption studies and presented in Figure 5. Inspection of the profiles reveals there is an initial rapid uptake of metal ions, but as time progresses the uptake slows and around the 150 minutes mark no further adsorption takes place. The quantity of metal ions adsorbed at equilibrium time (q_e) was determined by equation 2 below:

$$q_e = (C_o - C_e)\frac{V}{m} \quad (2)$$

where Co and Ce are the initial and equilibrium concentrations (mg/L) of metal ions in solution, V is solution volume (L) and m is absorber mass (g) used during the experiments. Three kinetic models were used to examine the experimental data. The first was the Lagergren pseudo-first order law [31] that is defined by equation 3 below:

$$\log(q_e - q_t) = \log q_e - \frac{k_1}{2.303}\,t \quad (3)$$

where, q_t (mg/g) is adsorption at time t and k1(min^{-1}) is the pseudo-first order adsorption rate constant. The second model used was the McKay and Ho's pseudo-second-order law [32] and is presented in equation 4:

$$\frac{t}{q_t} = \frac{1}{k_2 q_e^2} + \frac{1}{q_e}\,t \quad (4)$$

where k_2 (g/min.mg) is the pseudo-second-order rate constant for adsorption. The third model used was a multi-step intra-particle diffusion model proposed by Weber and Morris [33] and is defined by equation (5) below:

$$q_t = k_p\, t^{1/2} + C \quad (5)$$

where C is the intercept that provides the ideal boundary layer thickness and k_p is the intra-particle diffusion rate constant (mg/g.$min^{1/2}$ g).

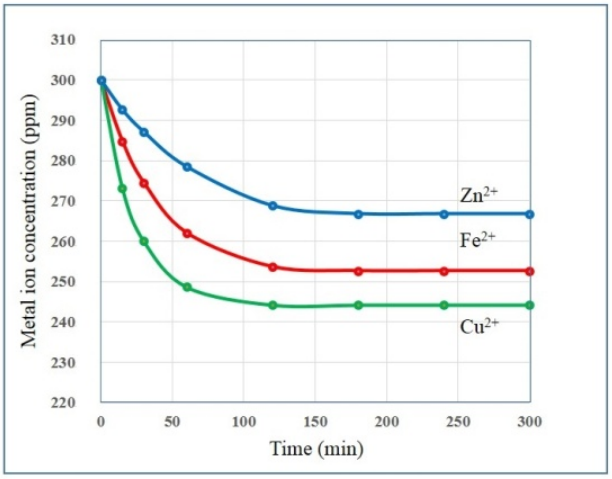

Figure 5. Metal ion concentration profiles during batch adsorption studies over a period of 300 minutes using a nanometre scale HAP powder as absorber

Figure 6 (a) presents kinetic data plotted using the Lagergren pseudo-first order equation (3), Figure 6 (b) displays the kinetic data plotted using the McKay and Ho's pseudo-second-order equation (4) and Figure 6 (c) represents the multi-gradient line data of intra-particle diffusion model (5). Inspection of Figures 6 (a) and (b) reveals that both the pseudo-first order and pseudo-second-order models gave reasonable representation of the data obtained. In spite of the good initial agreement, further analysis reveals the pseudo-second order model gives a better representation of the data for Fe^{2+} and Cu^{2+} ions with a slightly higher correlation coefficient (R^2) as seen in Table 1. However, in the case of Zn^{2+} ions, the intra-particle diffusion model gave a better representation of the data as seen in Figure 6 (c) and Table 1.

3.4. Adsorption Isotherms

There are two widely used equilibrium equations for modelling equilibrium data obtained from adsorption systems. The first model is the Freundlich and is purely an empirical equation that takes into account surface heterogeneity, the exponential distribution of active adsorption sites and their respective energies over a wide range of concentrations. The second model is the Langmuir equation and unlike the Freundlich, it assumes maximum adsorption occurs when the entire surface of the absorber is

covered by a monolayer of adsorbate. The equilibrium data for metal ions in solution for initial concentrations consisting of 100, 150, 200, 250 and 300 mg/L at constant temperature of 298 K, 1 g/L absorbent dose and a contact time of 300 minutes were analysed using Freundlich and Langmuir isotherms. The linear form of the Freundlich isotherm used for modelling the data is expressed by in equation (6):

$$\log q_e = \log k_F + \frac{1}{n} \log C_e \quad (6)$$

Table 1. A comparison between the pseudo kinetic (first and second order) rate constants and intra-particle kinetic diffusion constants

Pseudo-first-order kinetic model				
Metal ion	Temperature (K)	k_1 (min^{-1})	q_e (mg/g)	R^2
Fe^{2+}	298	33.92	55.24	0.9904
Cu^{2+}	298	19.99	62.50	0.9805
Zn^{2+}	298	115.53	57.14	0.9875
Pseudo-second-order kinetic model				
Metal ion	Temperature (K)	k_2 (g/mg.min)	q_e (mg/g)	R^2
Fe^{2+}	298	6.84 x 10^{-4}	52.91	0.9951
Cu^{2+}	298	12.15 x 10^{-4}	59.17	0.9980
Zn^{2+}	298	3.85 x10^{-4}	42.01	0.9734
Intra-particle kinetic diffusion model				
Metal ion	Temperature (K)	k_p (g/mg.min)	C (mg/g)	R^2
Fe^{2+}	298	4.29	1.12	0.9934
Cu^{2+}	298	4.17	13.17	0.9080
Zn^{2+}	298	3.77	-7.98	0.9995

where k_F and n are Freundlich parameters related to the extent of adsorption and the intensity of adsorption respectively. Both k_F and n parameters were determined via plotting log q_e versus log C_e , the results of which are presented in Figure 7 (a). The linear form of the Langmuir isotherm used for modelling the data is expressed by equation (7):

$$\frac{C_e}{q_e} = \frac{1}{Q_m\, b} + \frac{C_e}{Q_m} \quad (7)$$

where, Q_m (mg/g) is the monolayer adsorption capacity, b (L/g) is the Langmuir constant that is related to the free energy of adsorption, while C_e (mg/L) is the equilibrium concentration of adsorbate in solution and q_e (mg/g) is the concentration of adsorbate on the surface of absorber.

Both Q_{max} and b parameters were determined via plotting C_e/q_e versus C_e over the entire metal ion concentration range as seen in Figure 7 (b). The parameters reflect the surface properties and affinity of the metal ions for the nanometre scale HAP absorber. Both Langmuir and Freundlich plots exhibited good linear fits and were able to provide slope parameters and intercepts. The results of the respective isotherm analysis are listed in Table 2. For the Freundlich isotherm, if n falls within the range of 1 to 10 it indicates the adsorption process is favourable. In this study, n for all metal ions fell within this range and confirmed that adsorption was favourable. Furthermore, based on the coefficient of correlation (R^2) values, the Langmuir isotherm provided the best fit for Fe^{2+} and Cu^{2+} experimental data. While the Freundlich isothermal provided the best fit for Zn^{2+} experimental data. The maximum monolayer adsorption capacity (Q_m) for respective metal ions was calculated using the Langmuir equation and revealed the maximum adsorption capacity occurred for Cu^{2+} ions (61.35 mg/g). This was followed by Fe^{2+} ions (55.25 mg/g) and then Zn^{2+} ions (48.54 mg/g). The study also found that adsorption capacity was the result of increasing equilibrium metal ion concentrations in solution. The increased concentrations were able to increase the numbers of metal ions at the absorber surface and enhance the probability of adsorption.

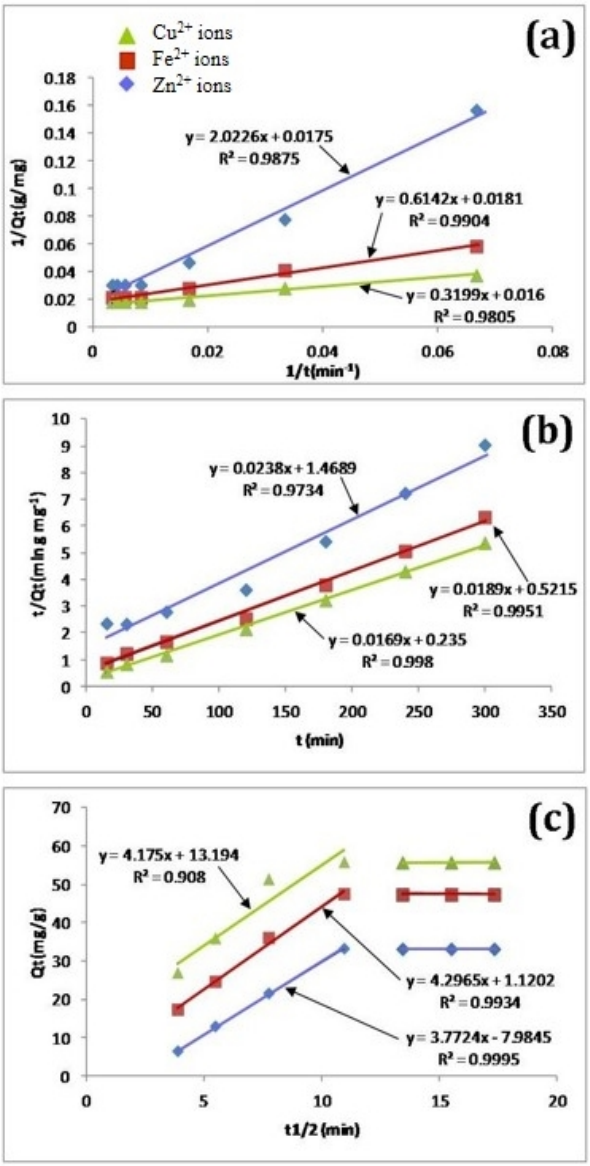

Figure 6. Metal ion adsorption data modelled using three kinetic models: (a) Lagergren's pseudo-first order law; (b) McKay and Ho's pseudo-second-order law, and (c) the intra-particle diffusion model

Table 2. Comparisons between Freundlich and Langmuir adsorption isotherm constants for metal ions (Fe^{2+}, Cu^{2+}, Zn^{2+}) onto nanometre scale hydroxyapatite at 298 K

Freundlich adsorption isotherm constants				
Metal ion	Temperature (K)	k_f (mg/g)	n	R^2
Fe^{2+}	298	19.02	5.685	0.9986
Cu^{2+}	298	21.17	5.640	0.9975
Zn^{2+}	298	3.53	2.448	0.9919
Langmuir adsorption isotherm constants				
Metal ion	Temperature (K)	Q_{max} (mg/g)	b (L/mg)	R^2
Fe^{2+}	298	55.25	0.036	0.9992
Cu^{2+}	298	61.35	0.038	0.9993
Zn^{2+}	298	48.54	0.009	0.9817

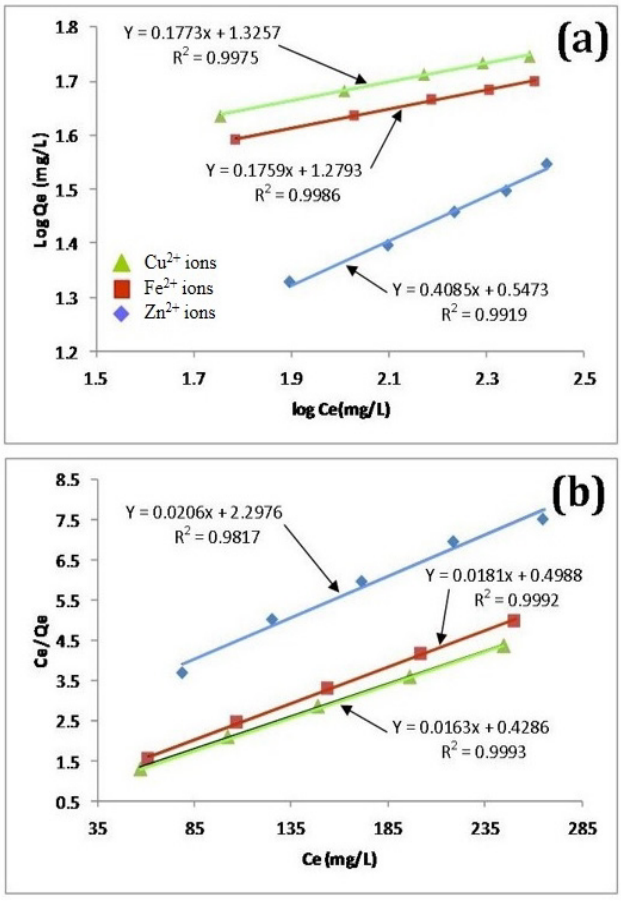

Figure 7. Linear fits of experimental data using (a) Freundlich and (b) Langmuir isotherms

Table 3 presents a comparison between the results of this study and with those reported in the literature for selected adsorbents. Comparing the adsorption capacity of HAP powder used in this study with the different adsorbents listed in Table 3 reveals the powder is an effective adsorbent for the removal of Fe^{2+}, Cu^{2+} and Zn^{2+} ions from aqueous solutions. Because of the relatively low-cost of the starting materials and the optimised ultrasound/microwave route used, the resultant HAP powder has the potential to be a cost-effective adsorbent for the removal of Fe^{2+}, Cu^{2+} and Zn^{2+} ions from aqueous solutions.

Table 3. Adsorption capacities for sorption of Fe^{2+}, Cu^{2+} and Zn^{2+} ions from aqueous solutions by various adsorbents

Adsorbent	**Q (mg/g)**			**Reference**
	Fe^{2+}	Cu^{2+}	Zn^{2+}	
Activated carbon derived from *Cicer arietinum*	-	17.77	19.93	34
Bentonite	-	14.10	21.1	35
Bone Charcoal	-	45.80	35.15	36
Cow Bone Charcoal	31.43	35.44	-	37
Egg Shell	-	34.48	35.71	38
Hydroxyapatite	-	36.9	-	39
Hydroxyapatite (30 nm)	55.25	61.35	48.54	This Study

4. Conclusions

The results of the present study have revealed that a nanometre scale HAP powder synthesized using a combined ultrasound and microwave based technique was capable of producing a highly crystalline powder consisting of spherical particle morphology with a mean particle size of 30 nm. The powder was found to be an effective adsorbent for the removal of metal ions such as Fe^{2+}, Cu^{2+} and Zn^{2+} from aqueous solutions. Kinetic studies revealed the sorption process for $Fe^{2+}$and Cu^{2+} ions closely followed pseudo-second order kinetics. While the slightly higher correlation coefficient (R2) of 0.9995 for Zn^{2+} ions indicated that the Intra-particle kinetic diffusion kinetics was more suited to modelling the experimental data. Overall, the sorption performance was found to be a function of initial metal ion concentration. With initial uptake rate of metal ions being high compared to the much lower uptake rates occurring in the later part of the absorption period. The ion-exchange mechanism (metal ion $\rightarrow$ Ca^{2+}) was seen to be a participant in the sorption process which was influenced by intra-particle diffusion. Isotherm studies indicated the Langmuir isotherm modelled Fe^{2+} and Cu^{2+} ion adsorption data better than the Freundlich isotherm. However, the Freundlich isotherm modelled the Zn^{2+} ion adsorption data. The Langmuir isotherm was used to determine maximum adsorption capacity of the HAP absorber for each metal ion. The study found the metal ion with the largest maximum adsorption capacity was Cu^{2+} ions (61.35 mg/g). This was followed by Fe^{2+} ions (55.25 mg/g) and then Zn^{2+} ions (48.54 mg/g).

ACKNOWLEDGEMENTS

Mrs Sridevi Brundavanam would like to acknowledge Murdoch University for providing a Postgraduate Scholarship to undertake this hydroxyapatite synthesis study as part of her PhD project.

REFERENCES

[1] Wongsasuluk, P., Chotpantarat, S., Siriwong, W., Robson, M., 2012, Heavy metal contamination and health risk assessment in drinking water from shallow groundwater wells in an agricultural area in Ubon Ratchathani province, Thailand, Environ Geochem Health, 36, 169-182.

[2] Jarup, L., 2003, Hazards of heavy metal contamination. British Medical Bulletin, 68 (1), 167-182.

[3] Babel, S., Kurniawan, T. A., 2004, Low-cost adsorbents for heavy metal uptake from contaminated water: a review, J. Hazard. Mater, B97, 219-243.

[4] Barakat, M. A., 2011, New trends in removing heavy metals from industrial waste water, Arabian Journal of Chemistry, 4, 361-377.

[5] Black, J., 1999, Biological performance of materials: Fundamentals of biocompatibility, Marcel Dekker, New York.

[6] Davis, J. R., 2003, Handbook of materials for medical devices. Materials Park, OH: ASM International.

[7] Hallab, N., Merritt, K., Jacobs, J. J., 2001, Metal Sensitivity in Patients with Orthopaedic Implants, J. Bone Joint Surg. Am., 83, 428-428.

[8] Lhotka, C., Szekeres, T., Steffan, I., Zhuber, K., Zweymuller, K., 2003, Four-year study of cobalt and chromium blood levels in patients managed with two different metal-on-metal total hip replacements, Journal of Orthopaedic Research, 21(2), 189-195.

[9] Haynes, D. R., Boyle, S. J., Rogers, S. D., Howie, D. W., Vernon-Robert, B., 1998, Variation in cytokines induced by patients from different prosthetic materials, Clinical Orthopaedics and Related Research, 352, 323-230.

[10] Geetha, M., Singh, A. K., Asokamani, R., Gogia, A. K., 2009, Ti based biomaterials, the ultimate choice for orthopaedic implants – A review, Progress in Materials Science, 54, 397–425.

[11] Kalita, S. J., Bhardwaj, A., Bhatt, H. A., 2007, Nanocrystalline calcium phosphate ceramics in biomedical engineering, Materials Science and Engineering C, 27(3), 441-449.

[12] Stoch, A., Jastrzebski, W., Dlugon, E., Lejda, W., 2005, Sol-gel derived hydroxyapatite coatings on titanium and its alloy Ti6Al4V, J Mol. Struct., 744-747, 633-640.

[13] Hutmacher, D. W., Schantz, J. T., Lam, C. X. F., Tan, K. C., Lim, T. C., 2007, State of the art and future directions of scaffold-based bone engineering from a biomaterials perspective, J. Tissue Eng. Regen. Med., 1, 245-260.

[14] Poinern, G. E. J., Brundavanam, R., Le, X., Nicholls, P. K., Cake, M. A., Fawcett, D., 2014, The synthesis, characterisation and in vivo study of a bioceramic for potential tissue regeneration applications, Scientific Reports, 4, 6235, 1-9.

[15] Cornell, C. N., Tyndall, D., Waller, S., Lane, J. M., Brause, B. D., 1993, Treatment of experimental osteomyelitis with antibiotic-impregnated bone graft substitute, J Orthop Res., 11(5), 619-626.

[16] Baro, M., Sanchez, E., Delgado, A., Perera, A., Evora, C., 2002, In vitro-in vivo characterisation of gentamicin bone implants, J Controlled Release, 83, 353-364.

[17] Ginebra, M. P., Traykova, T., Planell, J. A., 2006, Calcium phosphate cements as bone drug-delivery systems: a review, J Controlled Release, 113, 102-110.

[18] Schnieders, J., Gbureck, U., Thull, R., Kissel, T., 2006, Controlled release of gentamicin from calcium phosphate-poly (lactic acid-co-glycolic acid) composite bone cement, Biomaterials, 27, 4239-4249.

[19] Monteil-Rivera, F., Fedoroff, M., 2002, Sorption of inorganic species on apatite's from aqueous solutions: In Encyclopaedia of surface and colloid Science, Marcel Dekker, New York.

[20] Tanaka, H., Futaoka, M., Hino, R., Kandori, K., Ishikawa, T., 2005, Structure of synthetic calcium hydroxyapatite particles modified with pyrophosphoric acid, J. Colloid. Interface. Sci., 283, 609-612.

[21] Poinern, G. E. J., Brundavanam, R., Le, X., Djordjevic, S., Prokic, M., Fawcett, D., 2011, Thermal and ultrasonic influence in the formation of nanometre scale hydroxyapatite bio-ceramic, International Journal of Nanomedicine, 6, 2083-2095.

[22] Poinern, G .E. J., Brundavanam, R., Le, X., Fawcett, D., 2012, The mechanical properties of a porous ceramic derived from a 30 nm sized particles based powder of hydroxyapatite for potential hard tissue engineering applications. Am. J. Biomed. Eng., 2, 278-286.

[23] Klug, H. P., Alexander, L. E., 1974, X-ray diffraction procedures for poly-crystallite and amorphous materials. 2nd Ed., New York, Wiley.

[24] Barrett, C. S., Cohen, J. B., Faber, J., Jenkins, J. R., Leyden, D. E., Russ, J. C., Predecki, P. K., 1986, Advances in X-ray analysis, Vol. 29, New York: Plenum Press.

[25] Danilchenko, S. N., Kukharenko, O. G., Moseke, C., Protsenko, I. Y., Sukhodub, L. F., Sulkio-Cleff, B., 2002, Determination of the bone mineral crystallite size and lattice strain from diffraction line broadening, Cryst. Res. Technol., 37(11), 1234-1240.

[26] Ramesh, S. T., Rameshbabu, N., Gandhimathi, R., Nidheesh, P. V., Srikanth Kumar, M., 2012, Kinetics and equilibrium studies for the removal of heavy metals in both single and binary systems using hydroxyapatite, Appl. Water Sci., 2, 187–197.

[27] Evisa, Z., Yilmazb, B., Ustac, M., Aktugc, A. L., 2013, X-ray investigation of sintered cadmium doped hydroxyapatites, Ceramics International, 39, 2359–2363.

[28] Mobasherpour, I., Salahi, E., Pazouki, M., 2011, Removal of divalent cadmium cations by means of synthetic nano-crystallite hydroxyapatite, Desalination, 266, 142–148.

[29] Wang, Y., Zhang, S., Wei, K., Zhao, N., Chen, J., Wang, X., 2006, Hydrothermal synthesis of hydroxyapatite nano-powders using cationic surfactant as a template. Mater Lett., 60(12),1484-1487.

[30] Panda, R. N., Hsieh, M. F., Chung, R. J., Chin, T. S., 2003,

FTIR, XRD, SEM and solid state NMR investigations of carbonate-containing hydroxyapatite nano-particles synthesised by hydroxide-gel technique, J. Physics and Chemistry of Solids, 64(2), 193-199.

[31] Lagergren, S., 1893, Zur theorie der sogenannten adsorption gelöster stoffe, Kungliga Svenska Vetenskapsakademiens, Handlingar, 24, 1-39.

[32] McKay, G., Ho, Y. S., 1999, Pseudo-second order model for sorption processes, Process Biochem, 34, 451-465.

[33] Weber, W. J., Morris, J. C., 1963, Kinetics of adsorption on carbon from solution, J. Sanit. Engng. Div. Am. Soc. Civ. Engrs., 89, 31-60.

[34] Ramana, D. K. V., Jamuna, K., Satyanarayana, B., et al., 2010, Removal of heavy metals from aqueous solutions using activated carbon prepared from *Cicer arietinum,* Toxicological and Environmental Chemistry, 92, 1447-1460.

[35] Kubilay, A., Garkan, R., Savran, A., et al., 2007, Removal of Cu(II), Zn(II) and Co(II) ions from aqueous solutions by adsorption onto natural bentonite, Adsorption, 13, 41-51.

[36] Cheung, C. W., Porter, J. F., McKay, G., 2002, Removal of Cu(II) and Zn (II) ions by sorption onto bone char using batch agitation, Langmuir, 18, 650-656.

[37] Moreno, J. C., Gómez, R., Giraldo, L., 2010, Removal of Mn, Fe, Ni and Cu Ions from wastewater using cow bone charcoal, Materials, 3, 452-466.

[38] Putra, W. P., Kamari1, A., Yusoff, S. N. M., et al., 2014, Biosorption of Cu(II), Pb(II) and Zn(II) ions from aqueous solutions using selected waste materials: Adsorption and characterisation studies, Journal of Encapsulation and Adsorption Sciences, 4, 25-35.

[39] Wang, Y. J., Chen, J. H., Cui, Y. X., et al., 2009, Effects of low molecular weight organic acids on Cu (II) adsorption on hydroxyapatite nanoparticles, J Hazard Mater, 162, 1135-1140.